Analysis of triangular sharkskin profiles according to second law

Peter Liversage[1], Michele Trancossi[2*]

[1] Sheffield Hallam University, ACES Student, Sheffield, UK
[2] Sheffield Hallam University, Sheffield, UK - CEDITA by Romaero S.A. Bucharest, RO

Corresponding Author Email: mtrancossi@gmail.com

ABSTRACT

This paper presents the analysis of a case of sharkskin effect, caused by a turbulent flow over rough engineered surfaces. From a large bibliographic analysis, the paper describes the preliminary CFD simulations of a series of profiles such as sawtooth profile (12x6 mm), scalloped (R=6mm) and triangular (6x2 mm). Although a best solution has not been identified, different geometries and dimensions have been analysed and the initial results have shown the potential of a triangular profile with a 90° angle on top implemented on Coanda affected surfaces. The reference test profile adopted is an elevated surface with an inclined step placed upwind. The corrugated surface has been applied to analyse the coupled effect of sharkskin on both the viscous and pressure terms of drag. The results allow the assessment of a mathematical model of the sharkskin behaviour, assuming a continuous profile of the riblets. Results have also been assessed against a flat planar surface with the same measurements. The outcome has demonstrated a potential reduction up to 30% in the wall shear stress. The analysis has led to the formulation of a new equation to calculate the drag and lift force as a function of Bejan number. This model opens the possibility of applying a second law of analysis method to aerodynamic and fluid dynamic effects. Although this model has not been sufficiently demonstrated, it can allow a theoretical calculation of entropy generation in the case of the specific fluid dynamic phenomenon.

1. INTRODUCTION

Number of flights has increased by 80% between 1990 and 2014. Forecasts about air traffic trends expect a future growth by a further 45% between 2014 and 2035 [1-2]. Environmental impacts of aviation have increased over the past 25 years following the growth in air traffic (CO_2 emissions have increased by about 80%, NOX emissions have doubled between 1990 and 2014). They are expected to increase following the growth air traffic.

According to the energy consumption and emission figures, it is evident that a reduction of the aerodynamic vorticity would allow a major reduction of drag (up to 20%), which would bring large benefits to many engineering applications [3, 5] in aeronautics, ground and marine vehicles and pipelines.

Among several drag reduction methods that could be used are hydrophobic surfaces [6-8], compliant coatings [9-11], plasma actuators and dielectric barrier discharge [62-64], micro- bubbles injection [15-17] and riblets [18-20]. Riblets, wall grooves and sawtooth surfaces are highly attractive [21-25] because of their simplicity, low cost of manufacturing and easiness of maintenance.

The reduction of aerodynamic drag and boundary layer turbulence is facilitated by the roughness of the external shape and can be expressed in the function of Reynolds number (Kline et al. [26]; Robinson [27]; Yoon at al. [28-29]). Bechert [30], Reif [31] and Krieger [32] have observed that a surface, which emulates the skin of a shark, reduces the drag (Figure 1).
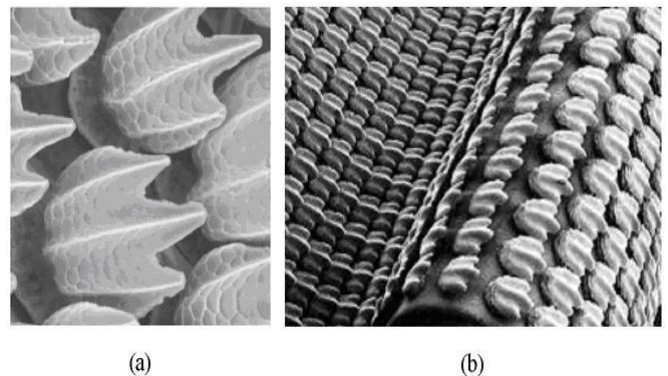

Figure 1. (a) real sharkskin; (b) artificial sharkskin by lauder with rigid denticles attached to a flexible membrane. (launder [83-84])

The following studies highlighted the positive effects on fluid adhesion of passive components:

(1) positive effects of riblets have been assessed by Walsh [33], Neumann [34], Rohr [35] and Lang [36];

(2) surface roughness in turbo machines has been studied by Kind [37], Hummel [38], and Dalili [39].

Walsh [40-43] has been the pioneer of the studies on drag reduction by riblets surfaces. He investigated the different behavior of bladed, scalloped and sawtooth surfaces, demonstrating that bladed riblets are the most efficient whilst sawtooth which have obtained a reduction of drag up to 8%.

Bechert et al. [44-45] have investigated more in depth different configurations of riblets and surfaces including rectangular, scalloped and shark-skin-shape riblets. They have conducted a deep experimental investigation on the methods for friction reduction effect using ribbed surfaces. Lee & Lee [46] have studied cross sectional vortexes above both flat-plate and semi-circular riblet surfaces by mean of flow visualization techniques. They have documented how the vortexes behave in both drag decreasing and drag increasing conditions; in particular, the effect of the spacing between the riblets. They have made the following observations: the drag reduces if most stream wise vortices stay above the riblets so the flow above the riblet valley is sufficiently calm; the drag, instead, increases if the riblet spacing is long enough to allow most stream wise vortices to stay inside the riblet valley (high-speed flows can penetrate into the riblet valleys).

Hubner [47-48], who focused on the trailing edge scalloping effect (Figure 2), has obtained results in line with Lee & Lee.
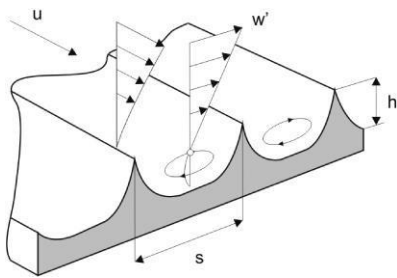

Figure 2. A typical profile of surface, vortex formation between teethes and fluid flow over the roughness [47]
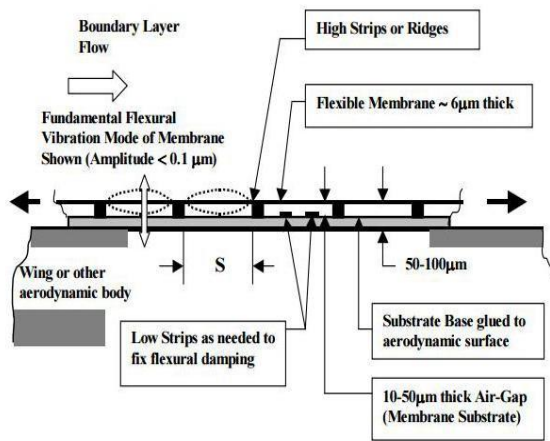

Figure 3. Sinha's composite deturbulator with composite flexible surface

Sinha [49-51] has studied a variable shape deturbulator taken from a composite deformable surface, made of a flexible membrane mounted on support ridges (Figure 3).

Büttner [52]'s studies of the effect of drag reduction due to riblet structured surfaces were originally inspired by shark scales, which have a drag reducing riblet structure. This activity has analyzed different technological possibilities for an adequate manufacturing in turbomachinery even in extreme conditions of pressure and temperature. Numerical simulations of turbulent flow have become an important tool for studying the basic physics of turbulence. For predicting the drag reduction with a riblet surface, most researchers use the Direct Numerical Simulation (DNS) method [53-56].

Choi et al. [55] numerically simulated the instantaneous turbulent structures over V-shaped riblets with s+=20 and s+=40 using DNS calculation and obtained results aligned with the experimental ones:

s$^+$=20 produced 5-6% drag reduction

s$^+$=40 produced a drag increase.

Although simulations by Reynolds-Averaged Navier-Stokes (RANS) models also have been completed by k-ε model and Reynolds Stress Model (RSM) model, these didn't give the expected results. Due to the difficulty in predicting correctly the drag variation when adopting isotropic models, like k-ε, one may choose other models to obtain the best results [56]. However, computational costs of DNS are high as it theoretically requires the mesh size to be smaller than the local Kolmogorov scale. In addition, a high Reynolds number leads to a smaller Kolmogorov scale in the flow and consequently, the grid amount may be beyond the capacity of computers, so the simulation is restricted to a low Reynolds number flow.

Research in the domain of biology and bioengineering has produced the definition of the sharkskin effect in terms of reduction of drag (Luchini [57]; Dean [58]; Bushan [59]). This research activity has produced new swimsuits that allow minimizing the skin friction during swimming activity (Toussaint [60]; Mollendorf [61]).

Anderson [62] has discovered that sharkskin produces a propulsive effect, which has been verified through experiments with mobile deformable substrate (Lang, Knight [63]).

2. METHODOLOGY

The proposed case differs slightly from existing literature. After a preliminary assessment of the parameters of CFD simulations, which have been reported in Appendix 1, the attention has been focused on 2D sawtooth profiles, which are schematized in Figure 4.
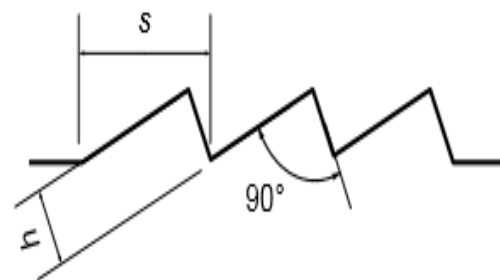

Figure 4. Sample of tested geometry profile

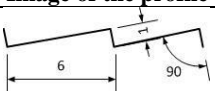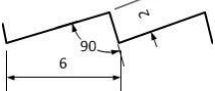The following geometries have been considered:
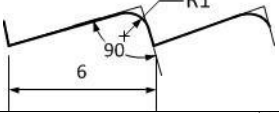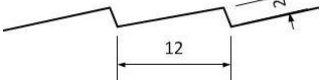1 x 6 mm, 2 x 6 mm,
3.5 x 6 mm,
2 x 12 mm,
2 x 6 R=1 mm (Table 1).

These profiles present a certain degree of novelty with respect to former literature both in terms of shape and in terms of expected results.

The proposed methodology will consider two types of fluid, which are water and air, in order to present an effective analysis.

Table 1. Different profiles analyzed

Dimensions h x s	Image of the profile
1 x 6 mm	
2 x 6 mm	
2 x 6 mm; R=1 mm	
2 x 12 mm	

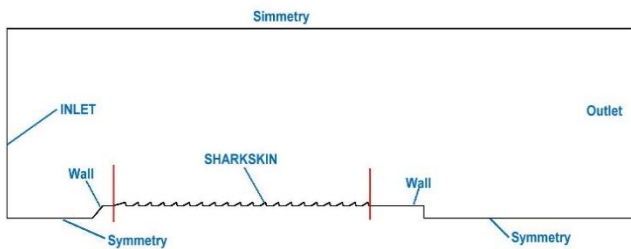A schema of the adopted computational domain has been presented in Figure 5.

Figure 5. Sample of the reference 2D domain

3. NUMERICAL MODELLING

Numerical modelling of the described phenomenon has been produced by CFD analysis in both 2D and 3D conditions. Two codes have been used for 2D and 3D Ansys fluent 17.1 Fluent v.17.1 (Spalart-Almaras and SST k-Ω) and Easy CFD (SST k-ε) for validation purposes of the 2D cases.
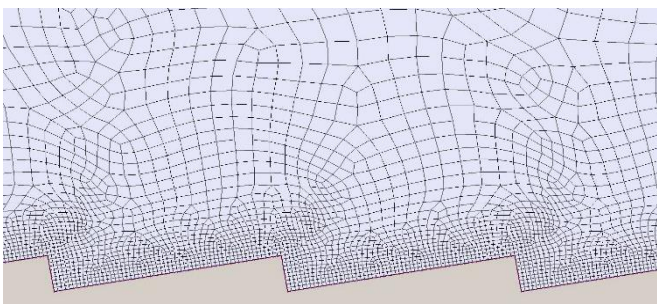

Figure 6. Sample of 2D mesh

2D analysis has been realized by means of quadrilateral mesh (Figure 6) and the results reported in Appendix 1.

A more effective 3D analysis has been performed by using a cut-cell square mesh.

In both cases, CFD simulations have been produced by using both Spalart-Almaras [64] and SST k-ε [65] turbulence model. The cut-cell grid has been produced in the Ansys Fluent 17.1 and the boundary layer resolved appropriately as shown in figure 7 and 8.
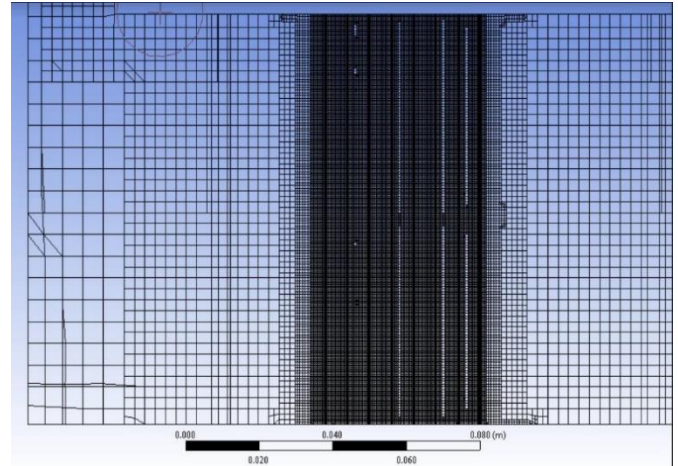

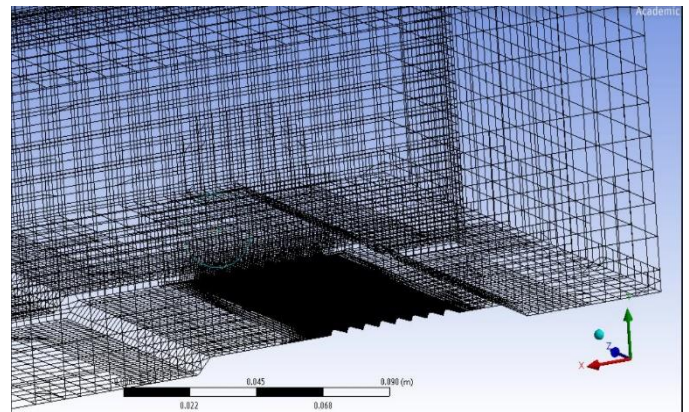**Figure 7.** Sample of 3D grid (to view)

Figure 8. General view of the cut cell 3D mesh

Grid independence check has been performed according to the ERCOFTAC [66] guidelines and as described in the following papers [67-69]. The optimum number of grid (numerically stable grid) has been determined through the numerical computation of the grid at different refinement levels. The final grid has allowed resolving the viscous sub-layer until a y+ value less than 2 and has leaded to identifying the stability conditions. The key characteristics of 2D and 3D meshes have been reported in Appendix 1.

Second order upwind scheme has been used to produce a discrete model of momentum equation and of k and ω model. The pressure and velocity have been coupled through the PISO (Pressure-Implicit with Splitting of Operators) method [70-71]. Pressure gradient term has been discretized by using the PRESTO (PREssure STaggering Option) method [72-73]. The PRESTO scheme has been used because it improves the pressure interpolation in situations where large body forces or strong pressure variation are present, including surface, geometry and thermal effects. To test the stability, a preliminary unsteady simulation has been used. It has been discretized by using first order implicit method taking advantage of unconditionally stable with respect to time step size, which has been as taken $\Delta t = 1 \times 10\text{-}03$ s.

4. RESULTS OF 2D SIMULATIONS

Simulations have been run using both water and air as fluid, due to the potential use of the proposed solution for

both ship hulls and aeronautic use. Fluid properties have been reported in Table 2.

Table 2. Fluid properties for the simulations

	Air at 15.0ºC	Water at 15.0ºC
Temperature (K)	288.15	288.15
Density (kg/m^3)	1.225	998
Viscosity (kg/m-s)	0.0000179	0.001003

The 2D results have been reported in table 3 and 4.

Table 3. Preliminary 2D results for water

5m/s water	L x H (mm)	Length (m)	wall shear stress (Pa)	τ Ratio	Re
shark (90∘)	6x1	0.12	0.10621	0.9650	613161
scalloped	12x2	0.12	0.07873	0.7153	613161
Saw tooth (60∘)	6x2	0.12	0.09831	0.8932	613161
smooth	n.a.	0.12	0.11006	1.0000	613161

Table 4. Preliminary 2D results for air

5m/s water	L x H (mm)	Length (m)	wall shear stress (Pa)	τ Ratio	Re
Shark (90∘)	6x1	0.12	0.00189547	0.9650	42102
scalloped	12x1	0.12	0.00150341	0.7654	42102
Sawtooth (60∘)	6x2	0.12	0.00185975	0.9468	42102
smooth	n.a.	0.12	0.00196421	1.0000	42102

It is evident that the preliminary 2D simulations produce a reduction of the wall shear stress between 5 and 30%.

The best solution is the scalloped case, as expected by literature analysis. The following analysis focuses on the triangular mesh profile, which has received a lower attention by current literature.
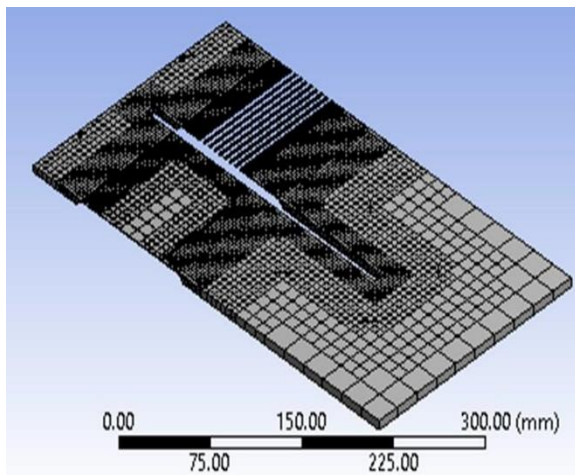

Figure 9. Boundary layer in the full 3D domain (on the left the flat plane and on the right the mesh of the rough profile

5. RESULTS OF 3D SIMULATIONS

Mesh properties and general samples of the results of the 3D simulations have been reported in Appendix 1.

The 3D domain used has been considered as composed by two different channels: The first being a flat surface and the other having roughness, allowing a good understanding of the boundary layer phenomena in presence and absence of the sharkskin. Air has been assumed for 3D simulations. Samples of velocity vectors, pressures in the 3D 6x2 mm, wall shear stress and turbulence structure have been reported in Appendix 1 and show some of the results obtained.

Figure 10 shows total drag of the three different profiles considered. Figure 11 shows the pressure component of the drag force, which appears in line with the expectations from 2D simulations. The high level of accuracy (10-9) on continuity has produced a good convergence of the results, which can be approximated by second order polynomials.
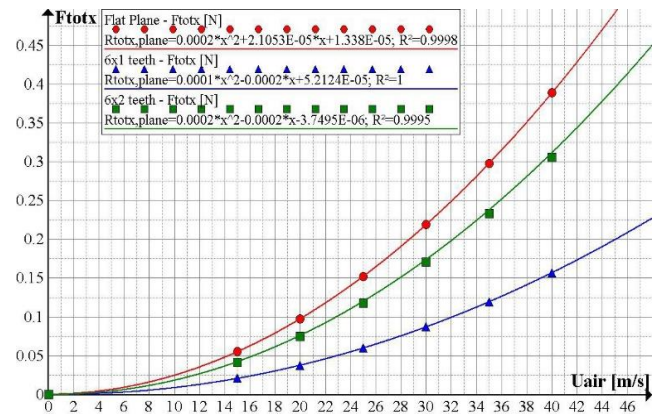
Figure 12 shows the viscous components.

Figure 10. Total force as a function of velocity
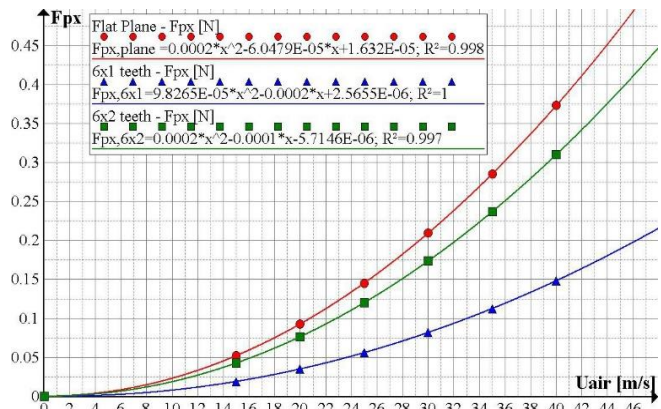
Figure 11. Pressure component of drag force

An apparently absurd result is shown in Figure 12. It seems due is due to the flow in configuration 6x2 presenting a negative viscous force. This can be explained by considering Figure 13, which highlights the structure of the vortex formation.

6. FURTHER THEORETICAL DISCUSSION

The results allow further theoretical considerations that involve the drag model and viscosity. It is necessary to define an effective model that can be used to describe the components of drag. The results are in line with the observations by Lauder et al. [75], Oeffner and Lauder [76], Knight [77] and Wen et al. [78-79] who have demonstrated the possibility of a propulsive effect by sharkskin if it fits some precise geometric parameters. The model is based on dimensionless parameters.

Figure 12. Viscous force
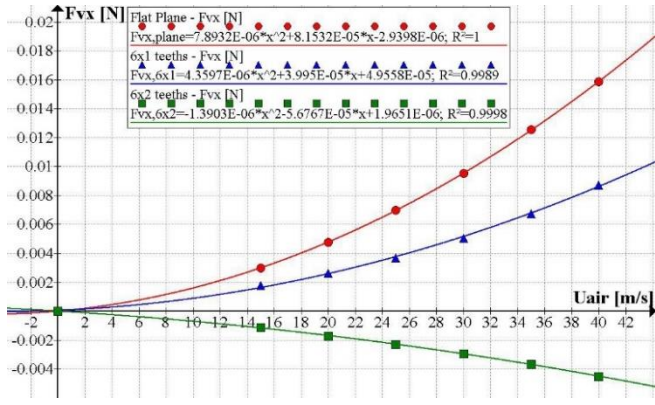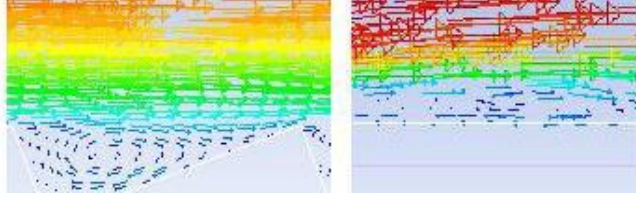

Figure 13. Detail of turbulence structure in 6x2 sharkskin profile and on a flat plane

The traditional expression of drag equation is:

$$D = \frac{1}{2} \cdot C_D \cdot A_f \cdot \rho \cdot u^2 \qquad (1)$$

Considering the definition of reynolds number, it becomes

$$D = \frac{1}{2} \cdot C_D \cdot A_f \cdot \frac{\mu^2}{\rho \cdot l^2} \cdot \frac{\rho^2 \cdot u^2 \cdot l^2}{\mu^2} = \frac{1}{2} \cdot C_D \cdot A_f \cdot \frac{\mu^2}{\rho \cdot l^2} \cdot \mathrm{Re}^2$$

Drag can be expressed as the change in pressure times the wet area A_w on which it is achieved.

$$\Delta p \cdot A_w = \frac{1}{2} \cdot C_D \cdot A_f \cdot \frac{\mu^2}{\rho \cdot l^2} \cdot \mathrm{Re}^2 \qquad (2)$$

In particular, by expressing C_D it becomes:

$$C_D = 2 \cdot \frac{A_w}{A_f} \cdot \frac{\Delta p \cdot \rho \cdot l^2}{\mu^2} \cdot \frac{1}{\mathrm{Re}^2} = 2 \cdot \frac{A_w}{A_f} \cdot \frac{\Delta p \cdot l^2}{\rho \cdot v^2} \cdot \frac{1}{\mathrm{Re}^2} \qquad (3)$$

The definition of Bejan number [80] has been extended to fluid-dynamic and convective problems by Mahmud [81, 82] and generalized by Avad [83]

$$Be = \frac{\Delta p \cdot l^2}{\rho \cdot v^2}$$

It allows producing a more compact and formulation of C_D:

$$C_D = 2 \cdot \frac{A_w}{A_f} \cdot \frac{Be}{\mathrm{Re}^2} \qquad (4)$$

The traditional formulation of Bejan number clearly shows that flow, irreversibility arises because of the combination of heat transfer phenomena and viscous effects of the fluid. In particular, it is defined as the ratio between the entropy generation by heat transfer and the total entropy generation during the motion of a fluid. The formulation proposed has been used into the field of external internal channel but is expected to fit well also with problems of external flows. If this formulation fits a more accurate verification, it could be possible to affirm that fluid-dynamic losses clearly belong to the thermodynamic domain of second principle. Considering that aerodynamic or hydrodynamic resistance can be considered as the composition of viscous component caused by shear stress and a pressure component caused by the modification of the streamlines caused by the presence of a body or by the external envelope, it is possible to produce a more effective formulation of the drag coefficient. The formulation proposed by Dumas [84] and Trancossi [85, 86] defines the fluid stream as subject to a difference of pressure that equilibrates the centrifugal force, which applies because of the rotation

$$\frac{\partial p}{\partial r} = \rho \cdot \omega^2 \cdot r = \rho \cdot \frac{u^2}{r} \qquad (5)$$

and to viscous effects that depends on the velocity

$$\tau = \mu \cdot \frac{\partial u}{\partial y} = c_f \cdot \frac{\rho \cdot u^2}{2}, \qquad (6)$$

in which c_f is a friction coefficient.

The above analysis of friction effects allows formulating a more detailed expression of equation (4)

$$C_D = 2 \cdot \frac{A_w}{A_f} \cdot \frac{Be_p + Be_v}{\mathrm{Re}^2} \qquad (7)$$

in which

$$Be_v = \frac{\Delta p_v \cdot l^2}{\rho \cdot v} \text{ and } Be_p = \frac{\Delta p_p \cdot l^2}{\rho \cdot v}$$

Equation 7 allows then to define two different drag coefficients that refer in detail to the two different phenomena that constitute drag:
a viscous component

$$C_{D,v} = 2 \cdot \frac{A_w}{A_f} \cdot \frac{Be_v}{\mathrm{Re}^2} \qquad (8)$$

a pressure component

$$C_{D,p} = 2 \cdot \frac{A_w}{A_f} \cdot \frac{Be_p}{\mathrm{Re}^2} \qquad (9)$$

This preliminary hypothesis has allowed producing an effective analysis at macroscopic scale of the specific aerodynamic phenomena and determining in detail the gain produced by sharkskin in different configurations.

It can be possible to consider the general formulation of the Bejan number as defined by Sciubba [87]:

$$Be = \frac{S'_{gen,\Delta T}}{S'_{gen,\Delta T} + S'_{gen,\Delta p}} \qquad (10)$$

Considering the phenomenon at domain level, according to Sciubba, it can be defined a global Bejan number with the following formulation

$$\overline{Be} = \frac{\int_{F*} S'_{gen,\Delta T} dF*}{\int_{F*} S'_{gen,\Delta T} dF* + \int_{F*} S'_{gen,\Delta p} dF*} \qquad (11)$$

We can assume the system is isothermal by neglecting the friction phenomenon that generates a small temperature difference. Viscous friction will generate a certain amount of heat, which is equal to the work of viscous drag.

In addition, it has been possible to evaluate the results in terms of second law and coupling specific aerodynamic phenomena and determining in detail the entropy generation produced by sharkskin in different configurations.
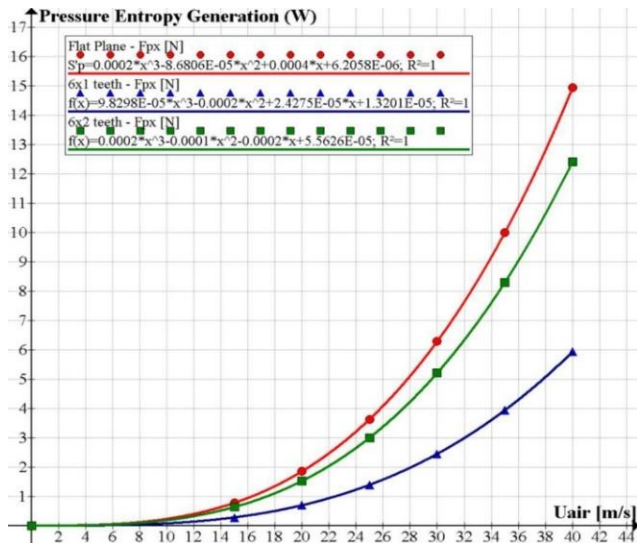

Figure 14. Entropy generation (pressure component)
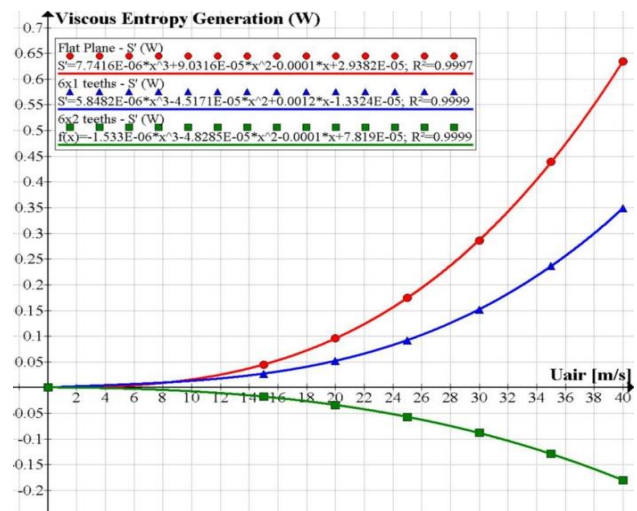

Figure 15. Entropy generation (viscous component)

By considering the original definition of Bejan Number in terms of ratio between entropic sources [88], it can be possible to produce an effective modelling of drag in terms of entropy generation. Drag is an entropic function and describes the entropy generation of a fluid with respect to boundaries or walls of an immerged body.

An accurate verification is required, but this hypothesis presents important margins of future development for modelling fluid dynamic problems in terms of second principle of thermodynamics. Entropy generation can then be evaluated by pressure (Figure 14) and viscous forces (Figure 15). The Drag coefficients have been evaluated (Figure 16). The results obtained are aligned with those determined numerically. Maximum error is 3%.
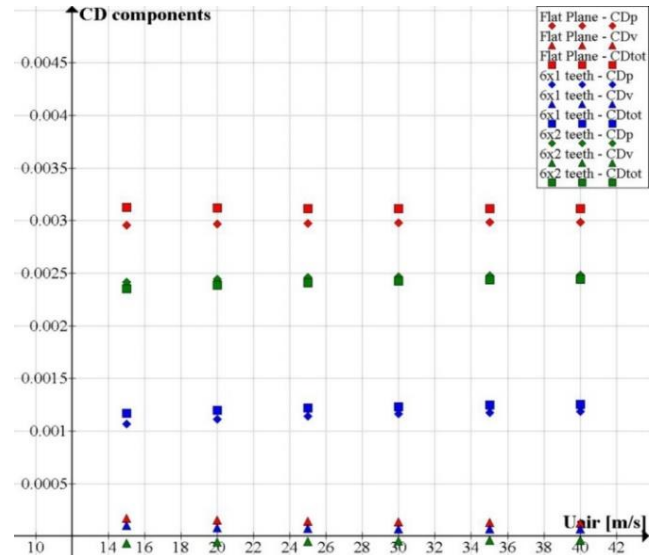

Figure 16. CD components

7. CONCLUSIONS

This paper presents the analysis of a case of sharkskin effect, which is caused by a turbulent flow over rough engineered surfaces. It presents the 2D simulations of some reference profiles, which has been used to tune the parameters of the following 3D simulations.

The preliminary results have evidenced the potential of a triangular profile with a 90° angle on top, which have been analysed considering different geometries and measures. They demonstrate clearly that sharkskin profiles can produce outstanding results in the reduction of wall shear stress. Results have been assessed against a flat plane with significant improvements up to 30%. These results are in line with the authors that claim the possibility of producing some positive thrust from the sharkskin effect. These results require a more accurate verification, which is currently being produced by both numerical and experimental activity.

The results have focused on the attempt of defining skin friction according to second law of thermodynamics, according to the preliminary formulation by Liversage [89]. Expressing the fluid dynamic phenomena in terms of Bejan number could be a possible research tool for the future. It has been possible to determine the entropy generation by both pressure and viscous drag components, by considering the definition of the Bejan number presented by Sciubba, These activities have an interesting potential for more effective

analysis of fluid dynamic phenomena.

REFERENCES

[1] Gierens K, Sausen R, Schumann U. (1999). A diagnostic study of the global distribution of contrails part II: Future air traffic scenarios. Theoretical and Applied Climatology 63(1): 1-9.

[2] Cheze B, Gastineau P, Chevallier J. (2010). Forecasting air traffic and corresponding jet-fuel demand until 2025. IFP Energies Nouvelles - IFP School - Centre economie et Gestion, France, IAEA. http://www.iaea.org/inis/collection/NCLCollectionStore/_Public/43/095/43095213.pdf?r=1

[3] Felder Wilson N, et al. (2017). Prospects for the application of practical drag reduction technologies to legacy transport aircraft. 55th AIAA Aerospace Sciences Meeting. https://doi.org/10.2514/6.2017-0044

[4] Wang Y, Wu C, Tan G, Deng Y. (2017). Reduction in the aerodynamic drag around a generic vehicle by using a non- smooth surface. Proceedings of the IMechE, Part D: Journal of Automobile Engineering 231(1): 130-144. https://doi.org/10.1177/0954407016636970

[5] Tardu S. (2017). Wall Turbulence Control, John Wiley & Sons. ISBN: 978-1-84821-559-7.

[6] Tian X, Verho T, Ras RH. (2016). Moving superhydrophobic surfaces toward real-world applications. Science. 352(6282): 142-143. https://doi.org/10.1126/science.aaf2073

[7] Bhushan B, Jung YC. (2011). Natural and biomimetic artificial surfaces for superhydrophobicity, self-cleaning, low adhesion, and drag reduction. Progress in Materials Science 56(1): 1-108. https://doi.org/10.1016/j.pmatsci.2010.04.003

[8] Koch K, Bohn HF, Barthlott W. (2009). Hierarchically sculptured plant surfaces and super hydrophobicity. Langmuir 25(24): 14116-14120. https://doi.org/10.1021/la9017322

[9] Klausmann K, Ruck B. (2017). Drag reduction of circular cylinders by porous coating on the leeward side. Journal of Fluid Mechanics 813: 382-411. https://doi.org/10.1017/jfm.2016.757

[10] Lee I, Boiko AV, Kulik VM. (2016). New perspective of turbulent skin friction reduction by compliant coating. Fluid- Structure-Sound Interactions and Control 133-138. Springer Berlin Heidelberg.

[11] Gad-el-Hak M. (2002). Compliant coatings for drag reduction. Progress in Aerospace Sciences 38(1): 77-99. https://doi.org/10.1016/S0376-0421(01)00020-3

[12] Rodrigues FF, Pascoa JC, Trancossi M. (2016). Analysis of innovative plasma actuator geometries for boundary layer control. ASME 2016 IMECE, ASME V001T03A007. doi:10.1115/IMECE2016-66495

[13] Corke TC, Enloe CL, Wilkinson SP. (2010). Dielectric barrier discharge plasma actuators for flow control. Annual Review of Fluid Mechanics 42: 505-529. https://doi.org/10.1146/annurev-fluid-121108-145550

[14] Versailles P, Gingras-Gosselin V, Vo HD. (2010). Impact of pressure and temperature on the performance of plasma actuators. AIAA journal 48(4): 859-863. https://doi.org/10.2514/1.43852

[15] Qin S, Chu N, Yao Y, Liu J, Huang B, Wu D. (2017). Stream-wise distribution of skin-friction drag reduction on a flat plate with bubble injection. Physics of Fluids 29(3): 037103. https://doi.org/10.1063/1.4977800

[16] Paik BG, Yim GT, Kim KY, Kim KS. (2016). The effects of microbubbles on skin friction in a turbulent boundary layer flow. International Journal of Multiphase Flow 80: 164-175. https://doi.org/10.1016/j.ijmultiphaseflow.2015.12.003

[17] Murai Y. (2014). Frictional drag reduction by bubble injection. Experiments in Fluids 55(7): 1773. https://doi.org/10.1007/s00348-014-1773-x

[18] Fu YF, Yuan CY, Bai XQ. (2017). Marine drag reduction of shark skin inspired riblet surfaces. Biosurface and Biotribology. https://doi.org/10.1016/j.bsbt.2017.02.001

[19] Hou J, Hokmabad BV, Ghaemi S. (2017). Three-dimensional measurement of turbulent flow over a riblet surface, Exp. Thermal and Fluid Science 85: 229-239. https://doi.org/10.1016/j.expthermflusci.2017.03.006

[20] Beyhaghi S, Amano RS. (2017). Slotted airfoils for increasing the aerodynamic efficiency. 55th AIAA Aerospace Sciences Meeting. 1839. https://doi.org/10.2514/6.2017-1839

[21] Sareen A, Deters RW, Henry SP, Selig MS. (2014). Drag reduction using riblet film applied to airfoils for wind turbines. Journal of Solar Energy Engineering 136(2): 021007. https://doi.org/10.1115/1.4024982

[22] Bixler GD, Bhushan B. (2013). Fluid drag reduction with shark skin riblet inspired microstructured surfaces. Adv. Functional Materials 23(36): 4507-4528. https://doi.org/10.1002/adfm.201203683

[23] West N, Sammut K, Tang Y. (2016). Material selection and manufacturing of riblets for drag reduction: An updated review. Proceedings of the Institution of Mechanical Engineers. Part L: Journal of Materials Design and Applications 1464420716641452. https://doi.org/10.1177/1464420716641452

[24] Luo Y, Xu X, Li D, Song W. (2015). Recent developments in fabricating drag reduction surfaces covering biological sharkskin morphology. Reviews in Chemical Engineering 32(1): 93-113. https://doi.org/10.1515/revce-2015-0015

[25] Luo Y, Wang J, Sun G, Li X, Liu Y. (2015). Experimental investigations on manufacturing different shaped bio-inspired drag reducing morphologies and hydrodynamic testing. Experimental Techniques. https://doi.org/10.1111/ext.12166

[26] Kline SJ, Reynolds WC, et al. (1967). The structure of turbulent boundary layers. J. Fluid Mech. 30: 741–773. https://doi.org/10.1017/S002211206700174

[27] Robinson, SK. (1991). The kinematics of turbulent boundary layer structure. NASA STI/Recon Technical Report N, 91, Washington, DC. http://adsabs.harvard.edu/abs/1991STIN.9126465R

[28] Yoon SH et al. (1993). Comparative study of a turbulent wall- attaching offset jet and a plane wall Jet. KSME 7: 101–112. https://doi.org/10.1007/BF02954360

[29] Yoon SH, Kim KC, et al. (1995). Effect of surface roughness on a turbulent wall-attaching offset jet. Experiments in Fluids 19: 38. doi:10.1007/BF00192231

[30] Bechert D, Reif W. (1985). On the drag reduction of the shark skin. In 23rd Aerospace Sciences Meeting p. 546. https://doi.org/10.2514/6.1985-546

[31] Krieger AIAA Journal, 21(4): 485-486. https://doi.org/10.2514/3.60126.

[32] Neumann D, Dinkelacker A. (1991). Drag measurements

on V-grooved surfaces on a body of revolution in axial flow. Applied Scientific Research 48(1): 105-114. https://doi.org/10.1007/BF01998668

[33] Robinson SK. (1991). The kinematics of turbulent boundary layer structure. NASA STI Tech. Report (91). http://adsabs.harvard.edu/abs/1991STIN.9126465R

[34] Lang AW, et al. (2008). Bristled sharkskin: a microgeometry for boundary layer control. Bioinspir. Biomim. 3: 1–9. https://doi.org/10.1088/1748-3182/3/4/046005

[35] Kind RJ, Serjak PJ, Abbott MW. (1998). Measurements and prediction of the effects of surface roughness on profile losses and deviation in a turbine cascade. Journal of Turbomachinery 120(1): 20-27. https://doi.org/10.1115/1.2841383

[36] Hummel F, et al. (2004). Surface roughness effects on turbine blade aerodynamics. Journal of Turbomachinery 127(3): 453-461. https://doi.org/10.1115/1.1860377

[37] Dalili N, Edrisy A, Carriveau R. (2009). A review of surface engineering issues critical to wind turbine performance. Renewable and Sustainable Energy Rev 13(2): 428-438. https://doi.org/10.1016/j.rser.2007.11.009

[38] Walsh MJ. (1980). Drag characteristics of V-groove and transverse curvature riblets. In AIAA Viscous Flow Drag Reduction 1979: 168-184. https://ntrs.nasa.gov/search.jsp?R=19810042106

[39] Walsh M. (1982). Turbulent boundary layer drag reduction using riblets. In 20th Aerospace Sciences Meeting 169. USA. https://doi.org/10.2514/6.1982-169

[40] Walsh MJ. (1983). Riblets as a viscous drag reduction technique. AIAA Journal 21(4): 485-486. https://doi.org/10.2514/3.60126

[41] Walsh MJ. (1990). Effect of detailed surface geometry on riblet drag reduction performance. Journal of Aircraft 27(6): 572- 573. https://doi.org/10.2514/3.25323

[42] Bechert DW, et al. (1997). Experiments on drag-reducing surfaces and their optimization with an adjustable geometry. Journal of Fluid Mechanics 338: 59-87. https://doi.org/10.1017/S0022112096004673

[43] Bechert DW, Bruse M, Hage W. (2000). Experiments with three- dimensional riblets as an idealized model of shark skin. Experiments in Fluids 28(5): 403-412. https://doi.org/10.1007/s003480050400

[44] Lee SJ, Lee SH. (2001). Flow field analysis of a turbulent boundary layer over a riblet surface. Exp. in Fl. 30(2): 153-166. https://doi.org/10.1007/s003480000150

[45] Hubner JP, Hicks T. (2011). Trailing-edge scalloping effect on flat-plate membrane wing performance. Aerospace Science and Technology 15(8): 670-680. https://doi.org/10.1016/j.ast.2011.01.004

[46] Hicks T, Conway M, Hubner JP. (2010). A study of trailing- edge scalloping on flat-plate membrane wing performance. In 48th AIAA Aerospace Sciences Meeting, AIAA Vol. 2070. https://doi.org/10.2514/6.2010-70

[47] Sinha SK, Ravande SV. (2006). Sailplane performance improvement using a flexible composite surface deturbulator. AIAA paper 447: 9-12. https://doi.org/10.2514/6.2006-447

[48] Sinha S, Sinha S. (2007). Improving automotive fuel efficiency with deturbulator tape. SAE Technical Paper 2007-01-3458. https://doi.org/10.4271/2007-01-3458

[49] Sinha SK, Hendrix J. (2009). Obtaining extremely high lift to drag ratios with flexible-wall turbulence control. 47th AIAA Aerospace Sciences Meeting, p. 896. https://doi.org/10.2514/6.2009-896

[50] Büttner CC, Schulz U. (2011). Shark skin inspired riblet structures as aerodynamically optimized high temperaturecoatings for blades of aeroengines. Smart Materials and Structures 20(9): 094016. https://doi.org/10.1088/0964- 1726/20/9/094016

[51] Goldstein D, Handler R, Sirovich L. (1995). Direct numerical simulation of turbulent flow over a modeled riblet covered surface. Journal of Fluid Mechanics 302: 333-376. https://doi.org/10.1017/S0022112095004125

[52] El-Samni OA, Chun HH, Yoon HS. (2007). Drag reduction of turbulent flow over thin rectangular riblets. Intl. J. of Engineering Science 45(2.8): 436-454. https://doi.org/10.1016/j.ijengsci.2007.03.002

[53] Choi H, Moin P, Kim J. (1993). Direct numerical simulation of turbulent flow over riblets. Journal of Fluid Mech 255: 503-539. https://doi.org/10.1017/S0022112093002575

[54] Benhamza M, Belaid F. (2009). Computation of turbulent channel flow with variable spacing riblets. Mechanika 5(79): 36-41.

[55] Luchini P, Manzo F, Pozzi A. (1991). Resistance of a grooved surface to parallel flow and cross-flow. J. Fluid Mech. 228: 87-109. https://doi.org/10.1017/S0022112091002641

[56] Krieger K. (2004). Do pool sharks swim faster?. Science, 305(5684): 636-638. https://doi.org/10.1126/science.305.5684.636

[57] Walsh MJ. (1983). Riblets as a viscous drag reduction technique. AIAA journal 21(4): 485-486. https://doi.org/10.2514/3.60126

[58] Dean B, Bhushan B. (2010). Shark-skin surfaces for fluid-drag reduction in turbulent flow: A review. Phil. Trans. of the Royal Society of London A: Mathematical, Physical and Engineering Sciences 368(1929): 4775-4806. https://doi.org/10.1098/rsta.2010.0201

[59] Bhushan B. (2012). Shark skin effect. In Encyclopedia of Nanotechnology 2400-2411. Springer Netherlands. ISBN 978-90-481-9751-4.

[60] Toussaint H, et al. (2002). Effect of a Fastskin bodysuit on drag during front crawl swimming. Intl. Soc. Biomech. Sports 1: 1-10. https://doi.org/10.1080/14763140208522783

[61] Mollendorf J, et al. (2004). Effect of swim suit design on passive drag. Med. Sci. Sports Exer. 36: 1029-1035. https://doi.org/10.1249/01.MSS.0000128179.02306.57

[62] Anderson EJ, McGillis W, Grosenbaugh MA. (2001). The boundary layer of swimming fish. J. Exp. Biol. 204: 81-102. http://jeb.biologists.org/content/204/1/81.short

[63] Knight, K. (2011). Shark skin produces propulsion. Journal of Experimental Biology 215(5). https://doi.org/10.1242/jeb.070698

[64] Spalart P, Allmaras S. (1992). A one-equation turbulence model for aerodynamic flows. In 30th Aerospace Sciences Meeting and Exhibit 439. https://doi.org/10.2514/6.1992-439

[65] Menter F. (1993). Zonal two equation kΩ turbulence models for aerodynamic flows, 23rd Fluid dynamics, plasmadynamics, and lasers conference 2906. https://doi.org/10.2514/6.1993-2906

[66] Casey M, Wintergerste T, Innotec S. (2000). ERCOFTAC special interest group on quality and trust in industrial CFD, Best practice guidelines.

www.ercoftac.org/downloads/pdfs/publications/bpg_contents_single-phase.pdf

[67] Oberkampf WL, Trucano TG. (2002). Verification and validation in computational fluid dynamics. Progress in Aerospace Sciences 38(3): 209-272. doi:10.1016/S0376-0421(02)00005-2

[68] Ashforth-Frost S, Jambunathan K. (1996). Numerical prediction of semi-confined jet impingement and comparison with experimental data. Int. J. for Num. Methods in Fluids 23(3): 295-306. https://doi.org/10.1002/(SICI)1097-0363(19960815)23:3<295::AID-FLD425>3.0.CO;2-T

[69] Kim JY, Ghajar AJ, Tang C, Foutch GL. (2005). Comparison of near-wall treatment methods for high Reynolds number backward-facing step flow. International Journal of Computational Fluid Dynamics 19(7): 493-500. https://doi.org/10.1080/10618560500502519

[70] Jang DS, Jetli R, Acharya S. (1986). Comparison of the PISO, SIMPLER, and SIMPLEC algorithms for the treatment of the pressure-velocity coupling in steady flow problems. Num. Heat Transf., Part A: Applications 10(3): 209-228. https://doi.org/10.1080/10407788608913517

[71] Wanik A, Schnell U. (1999). Some remarks on the PISO and SIMPLE algorithms for steady turbulent flow problems. Computers & Fluids 17(4): 555-570. https://doi.org/10.1016/0045-7930(89)90028-5

[72] Luo S, Heikkinen J, Roux B. (2004). Simulation of air flow in the IEA Annex 20 test room - validation of a simplified model for the nozzle diffuser in isothermal test cases. Building and Environment 39(12): 1403-1415. https://doi.org/10.1016/j.buildenv.2004.04.006

[73] Kumar A, Kim MH. (2015). Effect of roughness width ratios in discrete multi V-rib with staggered rib roughness on overall thermal performance of solar air channel. Solar Energy 119: 399-414. https://doi.org/10.1016/j.solener.2015.06.030

[74] Rizzi A, Vos J. (1998). Toward establishing credibility in computational fluid dynamics simulations. AIAA journal, 36(5): 668-675. https://doi.org/10.2514/2.442

[75] Tangorra J, Madden PG. (2007). Fish biorobotics: kinematics and hydrodynamics of self- propulsion. Journal of Experimental Biology 210(16): 2767-2780. https://doi.org/10.1242/jeb.000265

[76] Oeffner J, Lauder GV. (2012). The hydrodynamic function of shark skin and two biomimetic applications. Journal of Experimental Biology 215(5): 785-795. https://doi.org/10.1242/jeb.063040

[77] Knight K. (2012). Shark skin produces propulsion. Journal of Experimental Biology 215(5). https://doi.org/10.1242/jeb.070698

[78] Wen L, Weaver JC, Thornycroft PJ, Lauder GV. (2015). Hydrodynamic function of biomimetic shark skin: effect of denticle pattern and spacing. Bioinspiration & Biomimetics 10(6): 066010. https://doi.org/doi.org/10.1088/1748- 3190/10/6/066010

[79] Wen L, Weaver J, Lauder G. (2014). Biomimetic shark skin: design, fabrication and hydrodynamic function. Journal of Experimental Biology 217(10): 1656-1666. https://doi.org/10.1242/jeb.097097

[80] Bhattacharjee S, Grosshandler W. (1988). The formation of a wall jet near a high temperature wall under microgravity environment. Proceedings, ASME 1988 National Heat Transfer Conference, Houston, Tex., USA 1(A89-53251 23- 34): 711-716.

[81] Mahmud S, Fraser RA. (2002). Thermodynamic analysis of flow and heat transfer inside channel with two parallel plates. Exergy an International Journal 2(3): 140-146. https://doi.org/10.1016/S1164-0235(02)00062-6

[82] Mahmud S, Fraser RA. (2002). The second law analysis in fundamental convective heat transfer problems. Intl. J. of Th. Sci. 42(2): 177-186. https://doi.org/10.1016/S1290-0729(02)00017-0

[83] Awad MM, Lage JL. (2013). Extending the Bejan number to a general form. Thermal Science. 17(2): 631. https://doi.org/10.2298/TSCI130211032A

[84] Dumas A, Subhash M, Trancossi M, Marques JP. (2014). The influence of surface temperature on Coanda effect. Energy Procedia 45: 626-634. https://doi.org/10.1016/j.egypro.2014.01.067

[85] Trancossi M, Dumas A, Das SS, Pascoa J. (2014). Design methods of Coanda effect nozzle with two streams. INCAS Bulletin 6(1): 83. https://doi.org/10.13111/2066-8201.2014.6.1.8

[86] Trancossi M, Dumas A, Vucinic D. (2013). Mathematical modeling of Coanda effect. SAE Technical Paper, 2013-01-2195. https://doi.org/10.4271/2013-01-2195

[87] Sciubba E. A minimum entropy generation procedure for the discrete pseudo-optimization of finned-tube heat exchangers. Revue Generale de Thermique 35(416): 517-525. https://doi.org/10.1016/S0035-3159(99)80079-8

[88] Bejan A, Sciubba E. (1992). The optimal spacing of parallel plates cooled by forced convection. International Journal of Heat and Mass Transfer 35(12): 3259-3264. https://doi.org/10.1016/0017- 9310(92)90213-C

[89] Liversage P. Asymmetric characterisation of a shark-skin profile Beng (Hons) Sport Technology, Supervisor: Trancossi M. Department of Engineering & Mathematics, Sheffiled Hallam University, 2017.

NOMENCLATURE

CFD	Computational fluid Dynamics
Be	Bejan number
CD	Drag coefficient
Re	Reynolds number
Δt	Time step (s)
N	kinematic viscosity (cSt)
M	dynamic viscosity (cP)
P	Density (kg/m3)
T	shear stress (N/m2)
A	Area (m2)
D	Drag (N)
S'	Entropy (J)
P	pressure (Pa)
U	velocity (m/s)